

# The Role of Defects in Fe(II)–Goethite Electron Transfer

Luiza Notini,<sup>†</sup> Drew E. Latta,<sup>†</sup> Anke Neumann,<sup>‡</sup> Carolyn I. Pearce,<sup>§</sup> Michel Sassi,<sup>§</sup> Alpha T. N'Diaye,<sup>||</sup> Kevin M. Rosso,<sup>§</sup> and Michelle M. Scherer<sup>\*,†</sup>

<sup>†</sup>Department of Civil and Environmental Engineering, University of Iowa, Iowa City, Iowa 52242, United States

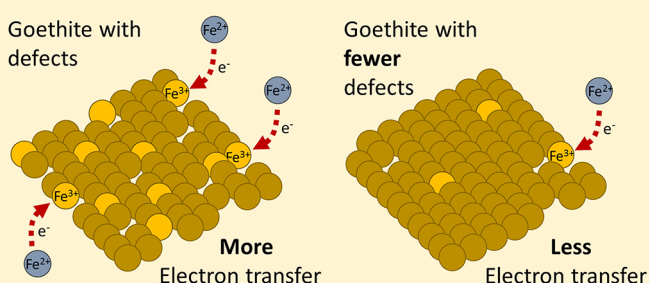
<sup>‡</sup>School of Engineering, Newcastle University, Newcastle upon Tyne, NE1 7RU, United Kingdom

<sup>§</sup>Pacific Northwest National Laboratory, Richland, Washington 99352, United States

<sup>||</sup>Advanced Light Source, Lawrence Berkeley National Laboratory, Berkeley, California 94720, United States

## Supporting Information

**ABSTRACT:** Despite substantial experimental evidence for Fe(II)–Fe(III) oxide electron transfer, computational chemistry calculations suggest that oxidation of sorbed Fe(II) by goethite is kinetically inhibited on structurally perfect surfaces. We used a combination of <sup>57</sup>Fe Mössbauer spectroscopy, synchrotron X-ray absorption and magnetic circular dichroism (XAS/XMCD) spectroscopies to investigate whether Fe(II)–goethite electron transfer is influenced by defects. Specifically, Fe L-edge and O K-edge XAS indicates that the outermost few Angstroms of goethite synthesized by low temperature Fe(III) hydrolysis is iron deficient relative to oxygen, suggesting the presence of defects from Fe vacancies. This nonstoichiometric goethite undergoes facile Fe(II)–Fe(III) oxide electron transfer, depositing additional goethite consistent with experimental precedent. Hydrothermal treatment of this goethite, however, appears to remove defects, decrease the amount of Fe(II) oxidation, and change the composition of the oxidation product. When hydrothermally treated goethite was ground, surface defect characteristics as well as the extent of electron transfer were largely restored. Our findings suggest that surface defects play a commanding role in Fe(II)–goethite redox interaction, as predicted by computational chemistry. Moreover, it suggests that, in the environment, the extent of this interaction will vary depending on diagenetic history, local redox conditions, as well as being subject to regeneration via seasonal fluctuations.



## INTRODUCTION

Ferrous and ferric iron comprise one of the most abundant redox couples, and electron transfer between these two oxidation states controls the cycling and availability of Fe in water, soil, and air.<sup>1,2</sup> Over the past decade significant evidence has accumulated to demonstrate interfacial electron transfer between sorbed Fe(II) and Fe(III) in Fe oxides and Fe-containing clay minerals.<sup>3–15</sup> In some cases, electron transfer also appears to be followed by mixing of Fe atoms from the bulk mineral structure with the surrounding fluid (also termed Fe(II)-catalyzed recrystallization).<sup>10,16–23</sup> While Fe(II)–Fe(III) electron transfer and mixing have been clearly demonstrated, a mechanistic understanding of these reactions remains elusive. Knowledge gaps in our understanding of Fe(II)–Fe(III) reaction mechanisms limit our ability to reliably predict important environmental and geochemical processes, such as cycling of C, N, and P,<sup>24–29</sup> water treatment,<sup>30</sup> contaminant remediation,<sup>31–34</sup> metal cycling,<sup>18,35</sup> mineral transformations,<sup>36</sup> and interpreting the ancient rock record.<sup>37</sup>

Thus far, Fe(II)–Fe(III) electron transfer has been demonstrated for several Fe oxides, including hematite, goethite, magnetite, ferrihydrite, as well as Fe-containing clay minerals.<sup>3–15</sup> Of the Fe minerals, electron transfer between Fe(II) and goethite has been the most extensively studied.

Oxidation of Fe(II) by goethite has been shown to occur over a range of Fe(II) concentrations, amounts of Al-substitution, and in the presence of various anions, such as phosphate, bicarbonate, silicate, and organic matter.<sup>3,4,6,8,10,12,16,17</sup>

Despite abundant experimental evidence for Fe(II)–Fe(III) oxide electron transfer, computational evidence suggests that Fe(II)–goethite electron transfer is not energetically favored on structurally perfect surfaces.<sup>38–40</sup> For example, density functional theory (DFT) calculations of Fe(II) adsorbed onto charge neutral, stoichiometric goethite (110) surfaces suggest that the oxidation of sorbed Fe(II) by lattice Fe(III) is energetically uphill. Others similarly conclude that charge only minimally delocalizes between Fe(II) and surface Fe(III), with only a minor dependence on the type of Fe(II)–mineral complex formed.<sup>39,40</sup> Additionally, a recent molecular dynamics study examining the electron transfer kinetics for stable inner and outer-sphere Fe(II) complexes on a wide range of perfect goethite terminations showed that the energetics are at best only thermoneutral, with large activation energies.<sup>41</sup>

**Received:** November 10, 2017

**Revised:** February 5, 2018

**Accepted:** February 6, 2018

**Published:** February 6, 2018



Each of these studies, however, suggest or infer that surface defects may underlie the experimentally observed interfacial electron transfer.<sup>38–40</sup> For example, calculations simulating an oxygen vacancy on goethite (110) showed that electron transfer to the resulting lower-coordinated Fe(III) was more energetically favorable and less kinetically inhibited. This idea is conceptually similar to the notion that defects provide traps in the interior of the solid for excess electrons to accumulate.<sup>9,42</sup> Given these computational findings, experiments designed to test the prospective role of defects could help advance our mechanistic understanding of Fe(II)–Fe(III) oxide electron transfer.

Defects arise from a deviation in the perfect composition and/or structure of a mineral. Such features are common in goethite<sup>43–47</sup> and have been previously studied in terms of their relationship to growth conditions,<sup>43,44,46,48</sup> including non-classical growth pathways such as imperfect oriented attachment.<sup>49–51</sup> The type and concentration of defects strongly influence goethite properties (e.g., *a*-dimension of the unit cell,<sup>43</sup> Néel temperature,<sup>47,52,53</sup> magnetic moment<sup>45,53–55</sup>) and particle reactivity (e.g., dissolution rates and ion sorption). Defects in the ideal goethite stoichiometry (i.e.,  $\alpha$ -FeOOH) can take the form of iron or oxygen vacancy, but often can be characterized as an excess of water/hydroxyl relative to the theoretical formula,<sup>46</sup> such that the effective formula is  $\alpha$ -Fe<sub>1–*y*/3</sub>O<sub>1–*y*</sub>(OH)<sub>1+*y*</sub>.<sup>43</sup> Changes in goethite properties after hydrothermal treatment have been interpreted to be due to removal of defects.<sup>43,44,56</sup> Conversely, ball-milling has been suggested to add defects to goethite based on observed changes in the Néel temperature.<sup>45</sup>

While there is clear evidence that defects are often present in goethite, little is known about how defects influence Fe(II)–goethite electron transfer. To date, no experimental data has been presented that specifically evaluates the role of defects in Fe(II)–goethite electron transfer, despite significant speculation about their role in enabling electron transfer and driving Fe(II)-catalyzed Fe oxide recrystallization.<sup>19,21,38–40</sup> Here we provide the first experimental evidence that shows defects influence the extent of Fe(II)–goethite electron transfer and the composition of the product formed. Our findings indicate that low temperature Fe(III) hydrolysis results in goethite particles that have excess hydroxyl/water content and corresponding Fe vacancies that enable Fe(II)–goethite electron transfer. Hydrothermally treating the goethite particles appears to remove defects, inhibit Fe(II)–goethite electron transfer, and alter the composition of the oxidation product. Our findings suggest that surface defects play an important role in Fe(II)–goethite redox interaction, as predicted by computational chemistry.

## MATERIALS AND METHODS

**Oxide Synthesis.** Goethite was prepared from <sup>56</sup>Fe-enriched Fe metal (Isoflex, 99.94% purity), <sup>56</sup>Fe goethite by modifying the Schwertmann and Cornell method, using iron metal as the synthesis' starting point instead of Fe(NO<sub>3</sub>)<sub>3</sub>.<sup>57</sup> Briefly, <sup>56</sup>Fe(0) was dissolved in HCl to obtain 15 mL of an Fe(II) stock (~0.6 M Fe(II), ~1.8 M HCl), and the solution was oxidized using 2 mL of 30% (slight excess) H<sub>2</sub>O<sub>2</sub> to produce Fe(III). Then, the pH was raised with 16 mL of 5 M KOH and the resulting precipitate was placed in an oven at 70 °C for 60 h. <sup>56</sup>Fe goethite was washed, centrifuged, freeze-dried, ground with a mortar and pestle, and passed through a 100 mesh sieve. The final mineral is referred to as “as-synthesized”

and it is similar to the microgoethite used in our previous work.<sup>3,6,10,12,16,17</sup> The Brunauer–Emmett–Teller (BET) specific surface area was determined by N<sub>2</sub> sorption at 77 K and found to be 28 to 34 m<sup>2</sup> g<sup>–1</sup>. X-ray diffraction (XRD - Rigaku Mini FlexII) patterns showed that the material contains goethite and no other minerals (Supporting Information (SI) Figure S7).

**Electron Transfer Experiments.** All experiments were carried out in an anaerobic glovebox with N<sub>2</sub>/H<sub>2</sub> atmosphere (93/7%), and all solutions were purged at least 2 h with N<sub>2</sub> prior to transfer into the glovebox. Fe(II) stock solutions were prepared inside the glovebox by reacting <sup>57</sup>Fe metal (Cambridge Isotope, 96.93% purity) with 1 M HCl overnight. The resulting solution was filtered to remove any residual Fe(0) and diluted with deionized (DI) water to the desired concentration (~100 mM Fe(II), ~0.1 M HCl).

Batch reactors were prepared by adding 10 mL of 25 mM HEPES (4-(2-hydroxyethyl)-1-piperazineethanesulfonic acid), pK<sub>a</sub> 7.55<sup>58</sup> buffer adjusted to pH 7.5 ± 0.05 plus 25 mM KBr electrolyte to a 20 mL glass vial and adding Fe(II) stock to reach an initial <sup>57</sup>Fe(II) concentration of ~1 mM. The reaction was started by adding 20.0 ± 0.2 mg of <sup>56</sup>Fe goethite and the reactors were placed on a end-over-end rotator in the absence of light. The aqueous phase was filtered (0.2 μm) and acidified with trace metal grade HCl for subsequent Fe(II) and total Fe analysis using the 1,10-phenanthroline method.<sup>59</sup>

**Extraction.** Two additional reactors were prepared by reacting <sup>56</sup>Fe goethite with <sup>57</sup>Fe(II), and the reacted solids were centrifuged and then extracted to remove the sorbed Fe species. The first reactor was extracted with a 0.4 M HCl (15 min). For the second reactor, the reacted solids were subjected to a sequential extraction procedure using HEPES buffer (pH 7.5, 1 h) followed by 1 M CaCl<sub>2</sub> (pH 7, 4 h) and 1 M NaH<sub>2</sub>PO<sub>4</sub> (pH 5, 18 h). A 30 min wash step with DI water was carried out after the CaCl<sub>2</sub> and NaH<sub>2</sub>PO<sub>4</sub>. The extracted solids were analyzed by Mössbauer spectroscopy and the extracted aqueous phase were analyzed for Fe(II) and total Fe.

**Hydrothermal Treatment.** Goethite was subjected to a hydrothermal treatment to anneal defects. A suspension of the as-synthesized <sup>56</sup>Fe goethite in deionized water was placed into a digestion bomb, and kept in an oven at 150 °C for 44 h. The digestion bomb was allowed to cool down and the solids were centrifuged and freeze-dried (referred to as hydrothermally treated goethite). The batch of hydrothermally treated goethite was split in two, and part of it was reacted with 1 mM <sup>57</sup>Fe(II) as discussed above. The other part was crushed with mortar and pestle to restore defects (referred to as ground goethite). Again, the batch was split, and part was reacted with 1 mM <sup>57</sup>Fe(II), while the other aliquot was hydrothermally treated again under the same conditions, and then reacted with 1 mM <sup>57</sup>Fe(II) (referred to as hydrothermally treated *again* goethite).

Samples of goethite after sequential treatments were characterized by XRD, scanning electron microscopy (SEM - Hitachi S-4800), transmission electron microscopy (TEM - JEOL JEM 1230), X-ray absorption spectroscopy (XAS) and X-ray magnetic circular dichroism spectroscopy (XMCD).

**Mössbauer Spectroscopy.** For Mössbauer spectroscopy, solids were collected on a 0.2 μm nitrocellulose filter and then sealed between two pieces of Kapton tape to avoid air oxidation. Mössbauer spectra were collected at 77 K on a spectrometer supplied by Web Research, Inc. (Edina, MN) and equipped with closed-cycle cryostat (CCS-850 System, Janis Research Co., Wilmington, MA). We acquired spectra in

transmission mode using a constant acceleration drive system and a  $^{57}\text{Co}$  source. The velocity scale was calibrated using a  $7\ \mu\text{m}$   $\alpha\text{-Fe}(0)$  foil. We fit the spectra using the software Recoil (Ottawa, Canada).<sup>60</sup>

Selected samples were reanalyzed after atmosphere exposure. After initial Mössbauer analysis, these samples were stored for a month in normal atmosphere and then reanalyzed by Mössbauer spectroscopy. For comparison, one sample was kept inside the anaerobic glovebox for the same time span.

**Synchrotron X-ray Absorption and Magnetic Circular Dichroism Spectroscopy.** For X-ray absorption spectroscopy, suspensions of goethite were dropped onto indium foil in an anaerobic glovebox with  $\text{N}_2/\text{H}_2$  atmosphere (93/7%), dried, then pressed into the foil and the excess solid was removed. The indium foil was attached to the copper sample manipulator with silver paint. XAS and XMCD measurements were performed using Beamline 6.3.1.1 at the Advanced Light Source (Berkeley, CA). Fe  $L_{2,3}$ -edge and O K-edge XAS were recorded at room temperature in total electron yield mode; Fe  $L_{2,3}$ -edge XAS has an effective probing depth of 50 Å. Fe  $L_{2,3}$ -edge XMCD spectra were obtained by measuring two XAS spectra with a fixed degree of circular polarization of  $\sim 0.7$  and with opposing magnetization directions by reversing the applied field of 1.8 T at each energy point. The XAS spectra were normalized to incident beam intensity, and the XMCD spectrum was obtained as the difference between the two spectra.

**Density Functional Theory Computations.** We used the FDMNES code<sup>61</sup> to individually calculate the O K-edge XANES spectra of the two oxygen sites present in goethite, explicitly taking into account their respective local coordination environments in the bulk structure. The Green's formalism approach, within the limit of the muffin-tin approximation, was used. The Fermi energy has been determined self-consistently using an aggregate of radii of 7 Å. A cluster of 7 Å radii has also been used to perform the final state calculations. The Hedin-Lundquist potentials<sup>62</sup> were used to model the exchange-correlation. Dipoles, core-hole contributions and spin-orbit coupling were taken into account. Because the experimental spectra of goethite is made of two components with unknown relative position and intensity, we have used a non-negative least-squares algorithm to refine the position and intensity of the two calculated  $\text{O}^{2-}$  and  $\text{OH}^-$  component spectra, and have found the best linear combination that would fit the experimental spectra. The resulting linear combination fit of the measured O K-edge spectra with the computed component spectra for  $\text{O}^{2-}$  and  $\text{OH}^-$  was used to quantify relative contributions of these two oxygen species.

## RESULTS AND DISCUSSION

**Fe(II)–Goethite Electron Transfer.** To explore if defects influence Fe(II)–goethite electron transfer, we ran a series of Fe isotope labeled experiments with as-synthesized and hydrothermally treated goethite particles. Similar to our previous work,<sup>3,5,6,10–12,14</sup> we took advantage of the element and isotope specificity of  $^{57}\text{Fe}$  Mössbauer spectroscopy to track if Fe(II)–goethite electron transfer occurs. Here, we treated Mössbauer-invisible  $^{56}\text{Fe}$  goethite with a sequence of hydrothermal treatment and grinding steps in an attempt to remove or add defects, presumably at surfaces, and then reacted the goethite with 1 mM  $^{57}\text{Fe}(\text{II})$  and collected  $^{57}\text{Fe}$  Mössbauer spectra of the filtered solids to determine if sorbed Fe(II) was oxidized (Figure 1). The  $^{57}\text{Fe}$  Mössbauer spectra of the reacted

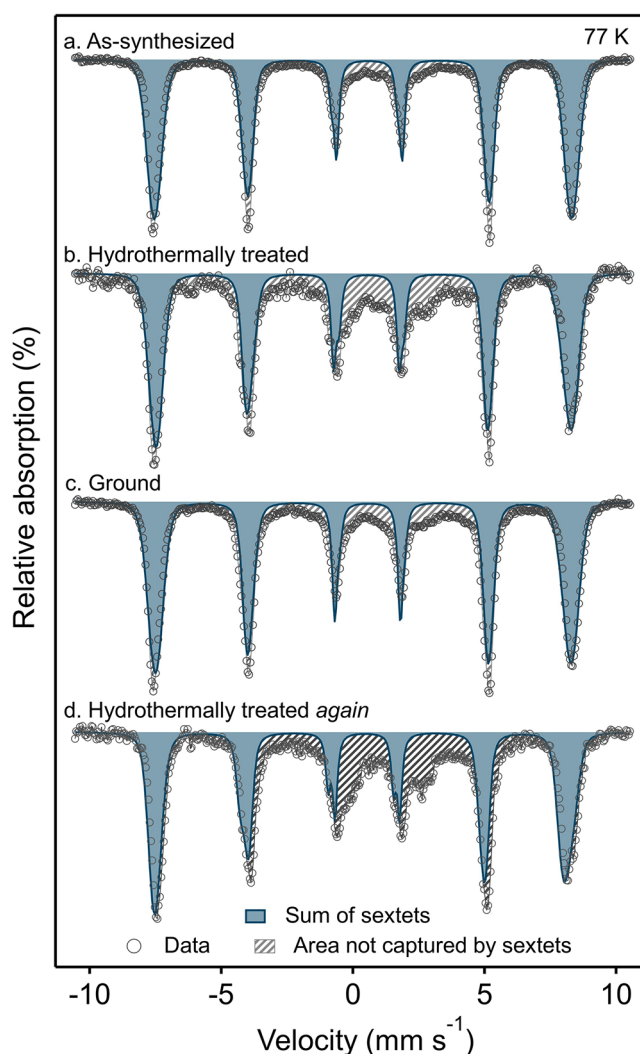


**Figure 1.** Mössbauer spectra of  $^{57}\text{Fe}(\text{II})$  reacted with  $^{56}\text{Fe}$  goethite after sequential hydrothermal/grinding treatments. Experimental conditions:  $[\text{Fe}^{2+}] = 2\ \text{g L}^{-1}$ , 25 mM HEPES/25 mM KBr at pH 7.5.

solids revealed two prominent Fe(III) sextets consistent with goethite and suggest that substantial oxidation of  $^{57}\text{Fe}(\text{II})$  occurred and formed  $^{57}\text{Fe}$  goethite on both the as-synthesized goethite and the hydrothermally treated goethite (SI Table S1). Oxidation of sorbed Fe(II) by goethite is consistent with our and others' previous work.<sup>3,6,8,10,12</sup>

After reaction with  $^{57}\text{Fe}(\text{II})$ , there is, however, a marked difference between the as-synthesized goethite and the hydrothermally treated goethite. The Fe(III) sextets capture a smaller portion of the spectral area of the hydrothermally treated compared to the as-synthesized goethite (as shown by blue sextets in Figure 1a and b). To test if the change in spectral area distribution upon hydrothermal treatment was reversible, we ground the hydrothermally treated goethite particles and reacted them with  $^{57}\text{Fe}(\text{II})$ . The resulting spectrum shows a marked increase in the amount of area captured by the sextet (and less hatched area) (Figure 1c). A second hydrothermal treatment returned the spectrum of Fe(II)-reacted solids to one similar to that of the first hydrothermal treatment (Figure 1d). To test that the change in spectral area trend observed in Figure 1 was not particular to a goethite synthesis batch, we ran duplicates of each treatment using two separate batches of goethite (SI Figure S1). The



similarity of the duplicate experiments conducted with two separately synthesized goethite batches provides strong evidence that hydrothermal treatment and grinding are reproducibly altering the goethite in a way that influences how it reacts with Fe(II).

The reversible, reproducible changes in the Mössbauer spectra indicate that hydrothermal treatment and grinding are influencing the product formed from  $^{57}\text{Fe(II)}$  interaction with goethite. To fit the hatched area in the Mössbauer spectra we tried a variety of approaches. We concluded that the best method to capture the hatched area was to include an Fe(II) doublet and a broad, collapsed sextet consistent with our and other's previous approach (for more details see SI Figure S2).<sup>10,63</sup> Small Fe(II) doublets comprising less than 10% of the total area have been previously observed in spectra of goethite reacted with  $^{57}\text{Fe(II)}$ ,<sup>8,10,12</sup> but little is known about the composition of the broad, collapsed sextet and we have, in our previous work, been careful to not interpret it beyond that it was likely Fe(III).<sup>10</sup> To check whether that the collapsed feature was influenced by buffer–Fe interactions,<sup>64</sup> we ran a control experiment without buffer (SI Figure S4). There was no difference between the spectra of the buffered and unbuffered samples indicating that the buffer–Fe interactions were not responsible for the collapsed feature.

To investigate the composition of the collapsed feature, we subjected the as-synthesized goethite particles reacted with  $^{57}\text{Fe(II)}$  to different extraction procedures and collected Mössbauer spectra afterward (Figure 2). A mild HCl extraction (0.4 M) removed both the Fe(II) doublet and the broad, collapsed sextet from the Mössbauer spectra. All of the Fe(II) that had initially sorbed was recovered in the HCl extract (SI Table S2). Surprisingly, the aqueous extract from the HCl treatment contained only Fe(II), suggesting that the collapsed feature was at least partially due to Fe(II). To minimize the change in pH during extraction, we also extracted goethite reacted with  $^{57}\text{Fe(II)}$  with  $\text{CaCl}_2$  and  $\text{NaH}_2\text{PO}_4$  which only decreased the pH to 7 and 5, respectively. Similar to the HCl extraction, the milder extractions removed most of the collapsed feature and recovered similar amounts of Fe(II) (for additional discussion see SI Figure S5).

As an alternative approach to evaluate whether the collapsed feature contains Fe(II), we oxidized a sample of goethite reacted with  $^{57}\text{Fe(II)}$  to see if the collapsed feature disappeared. One month of air exposure resulted in complete removal of the collapsed feature and the Fe(II) doublet from the spectra, providing an additional line of evidence that the collapsed feature contained some Fe(II) (Figure 2). The spectra of the oxidized goethite, however, looks slightly different than the spectra of the HCl-extracted goethite, in which a third sextet appeared. The third sextet was identified as akaganéite, a mineral typically formed by the hydrolysis of Fe(III) salts in the presence of  $\text{Cl}^-$ .<sup>65</sup> Regardless of the precise identity of the collapsed feature, the oxidation and extraction data combined provide compelling evidence that the collapsed feature contains some Fe(II) and is more likely a mixed Fe(II)–Fe(III) phase rather than a pure Fe(III) phase as we previously thought.<sup>10</sup> While we cannot rule out that it is a pure Fe(II) phase, the Mössbauer parameters of the collapsed sextet are more consistent with a mixed Fe(II)–Fe(III) compound (further discussed in the SI).<sup>66</sup> Importantly, the presence of a mixed Fe(II)–Fe(III) phase rather than an Fe(III) phase suggests that some of  $^{57}\text{Fe(II)}$  sorbed on goethite was not oxidized by the goethite.

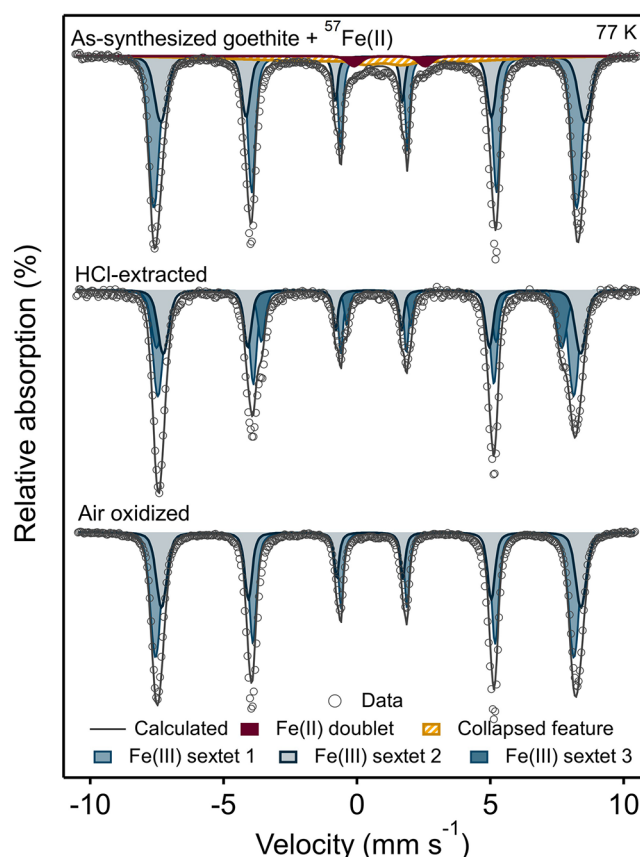


**Figure 2.** Mössbauer spectra of  $^{56}\text{Fe}$  as-synthesized goethite reacted with 1 mM  $^{57}\text{Fe(II)}$ , before and after HCl extraction and air oxidation. Experimental conditions:  $[\text{Gt}] = 2 \text{ g L}^{-1}$ , 25 mM HEPES/25 mM KBr at pH 7.5.

To quantify the extent of sorbed Fe(II) that was oxidized to goethite as a function of surface treatment, we plotted the percent relative area of the two goethite sextets for the as-synthesized goethite and the successive hydrothermally treated and ground goethite particles (Figure 3). If one hundred percent of the spectral area was captured within the two

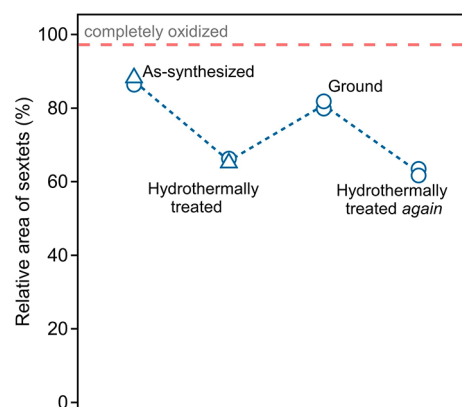


**Figure 3.** Relative area of Fe(III) sextets from Mössbauer spectra of  $^{57}\text{Fe(II)}$  reacted with  $^{56}\text{Fe}$  goethite after sequential hydrothermal/grinding treatments. Percentages based on spectral fits shown in SI Figure S2 (data in Table S1) and described in the SI. Different markers indicate different  $^{56}\text{Fe}$  goethite batches. Duplicates from the same batch were hydrothermally treated/ground in separate experiments.

goethite sextets, it would indicate that all of the sorbed  $^{57}\text{Fe}(\text{II})$  was oxidized to  $^{57}\text{Fe}(\text{III})$  goethite. Complete oxidation of  $\text{Fe}(\text{II})$  did not occur in any of the samples, but instead the amount of  $\text{Fe}(\text{II})$  oxidized to form goethite varied between 63 and 87% (as estimated from the relative area of the sextets). What is most striking in Figure 3, however, is how reversible and reproducible the hydrothermal and grinding treatment is in influencing the extent of oxidation of the goethite-sorbed  $\text{Fe}(\text{II})$ . The as-synthesized goethite oxidized  $\approx 87\%$  of the sorbed  $\text{Fe}(\text{II})$  to form goethite, whereas hydrothermally treating the goethite particles resulted in only  $\approx 66\%$  of the sorbed  $^{57}\text{Fe}(\text{II})$  becoming oxidized to goethite, suggesting that electron transfer was inhibited by hydrothermal treatment and that the composition of the oxidation product changed. Grinding the hydrothermally treated goethite largely restored the extent of electron transfer ( $\approx 81\%$ ), and hydrothermally treating this goethite sample *again* inhibited the extent of electron transfer ( $\approx 63\%$ ) (Figure 3).

Similar to the as-synthesized goethite, one month of air exposure of the hydrothermally treated goethites resulted in removal of the collapsed feature and the  $\text{Fe}(\text{II})$  doublets from the spectra, consistent with the collapsed feature containing some  $\text{Fe}(\text{II})$  (SI Figure S6). The hydrothermally treated goethites reacted with  $^{57}\text{Fe}(\text{II})$  also lost substantially more spectral area than the ground samples (as-synthesized and ground goethite), providing additional evidence that hydrothermally treating goethite leads to less oxidation of sorbed  $\text{Fe}(\text{II})$  to goethite.

**Bulk Characterization of Goethite Particles.** It appears that hydrothermal treatment and grinding reversibly and reproducibly influences the extent of electron transfer from sorbed  $\text{Fe}(\text{II})$  to goethite as well as the composition of the oxidation product. Given previous evidence that goethite synthesis conditions such as temperature alter the defect content in goethite,<sup>43,44</sup> we hypothesized that hydrothermally treating the goethite particles at  $150\text{ }^{\circ}\text{C}$  annealed defects present in the goethite synthesized at  $70\text{ }^{\circ}\text{C}$ . We further hypothesized that grinding the particles added defects back to the hydrothermally treated particles. To evaluate if there were any changes in the bulk goethite particles before and after treatments, we characterized the particles with XRD, BET analysis, and microscopy. XRD spectra of treated solids confirmed that hydrothermal treatment did not transform goethite into any other mineral (SI Figure S7), and cell dimensions were unchanged after the goethite sequential hydrothermal/grinding treatments (SI Table S3). Schwertmann and collaborators observed a slight change in the  $a$ -axis dimension upon hydrothermal treatment, however, their initial material was a highly defective goethite.<sup>43</sup> BET measurements revealed a small, but progressive loss in BET area (from  $28$  to  $19\text{ m}^2\text{ g}^{-1}$ , SI Table S3), consistent with previous observations.<sup>43,44,56</sup> In our work, TEM images revealed no substantial difference between as-synthesized and hydrothermally treated goethite, but SEM images revealed slight changes of the surface (SI Figure S8 and S9). Hydrothermally treated goethite appeared to have more perfectly formed ends when compared to the original mineral suggesting the hydrothermal treatment may have removed some surface defects (SI Figure S9).

Because hydrothermal treatment resulted in smaller BET surface area and amounts of  $\text{Fe}(\text{II})$  sorbed, we considered the alternative hypothesis that less  $\text{Fe}(\text{II})$ –goethite electron transfer could be simply due to less surface area and less

surface-bound  $\text{Fe}(\text{II})$  available to be oxidized. To explore whether the amount of sorbed  $\text{Fe}(\text{II})$  influenced the extent of electron transfer, we plotted the percent relative area of the  $\text{Fe}(\text{III})$  sextets versus sorbed  $\text{Fe}(\text{II})$  per  $\text{m}^2$  (Figure 4). We

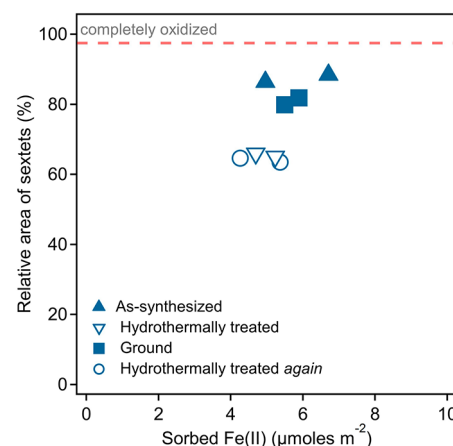


**Figure 4.** Relative area of  $\text{Fe}(\text{III})$  sextets from Mössbauer spectra as a function of sorbed  $\text{Fe}(\text{II})$  per  $\text{m}^2$  for samples of  $^{57}\text{Fe}(\text{II})$  reacted with goethite after sequential hydrothermal/grinding treatments.

binned the data into ground goethites which includes as-synthesized and ground (solid markers) and hydrothermally treated goethites which includes both rounds of hydrothermal treatment (open markers). Both ground and hydrothermally treated goethites converge to  $\sim 5.5\text{ }\mu\text{moles Fe}(\text{II})$  sorbed per  $\text{m}^2$ , revealing that the sorption of  $\text{Fe}(\text{II})$  was not influenced by the treatment applied to the mineral. However, it is remarkable that, when we compare a hydrothermally treated and a ground goethite that have the same amount of  $\text{Fe}(\text{II})$  sorbed per  $\text{m}^2$ , there is a marked difference ( $\approx 20\%$ ) in the extent of electron transfer. Figure 4 provides compelling evidence that the changes we observed in  $\text{Fe}(\text{II})$ –goethite electron transfer between our four treatments were not due to changes in surface area or amount of  $\text{Fe}(\text{II})$  sorbed.

**Surface Characterization of Defects on Goethite Particles.** While bulk characterization of the treated goethite particles is informative, it is unlikely we would be able to detect specific changes in goethite surface structure with these techniques. To detect the presence of defects and changes in surface structure in the treated goethites, we collected X-ray absorption spectroscopy (XAS) and X-ray magnetic circular dichroism (XMCD) at the  $\text{Fe L}$ -edge and XAS at the  $\text{O K}$ -edge. By collecting total electron yield data, these techniques probe a depth no greater than  $5\text{ nm}$  and are mainly sensitive to the upper few Angstroms.<sup>67</sup>  $\text{Fe L}$ -edge XMCD spectra for all three samples is shown in Figure 5, while the illustrative  $\text{O K}$ -edge spectra and DFT-based spectral analysis are shown in Figure 6.

The  $\text{Fe L}$ -edge XAS probes the structure and valence of surface iron, whereas the XMCD is selective for the subset of surface iron that is magnetically ordered and is able to discriminate  $\text{Fe}$  valence and local coordination. As expected, the  $\text{Fe L}$ -edge XAS of all goethite samples measured shows features consistent with goethite  $\text{Fe}(\text{III})$ ;  $\text{Fe}(\text{II})$  is not detected (SI Figure S10). The corresponding XMCD information, however, is more revealing (Figure 5). The as-synthesized goethite has a weak magnetic moment at the surface (i.e., from the magnetic dichroism signal intensity), and the shape of the XMCD signal is consistent with octahedrally coordinated  $\text{Fe}(\text{III})$ .<sup>68</sup> The

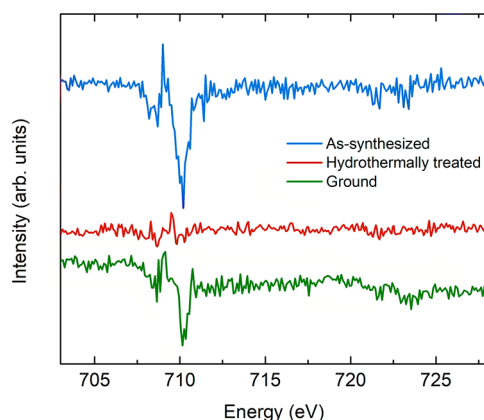


**Figure 5.** Fe L-edge XMCD of goethite after sequential hydrothermal/grinding treatments.

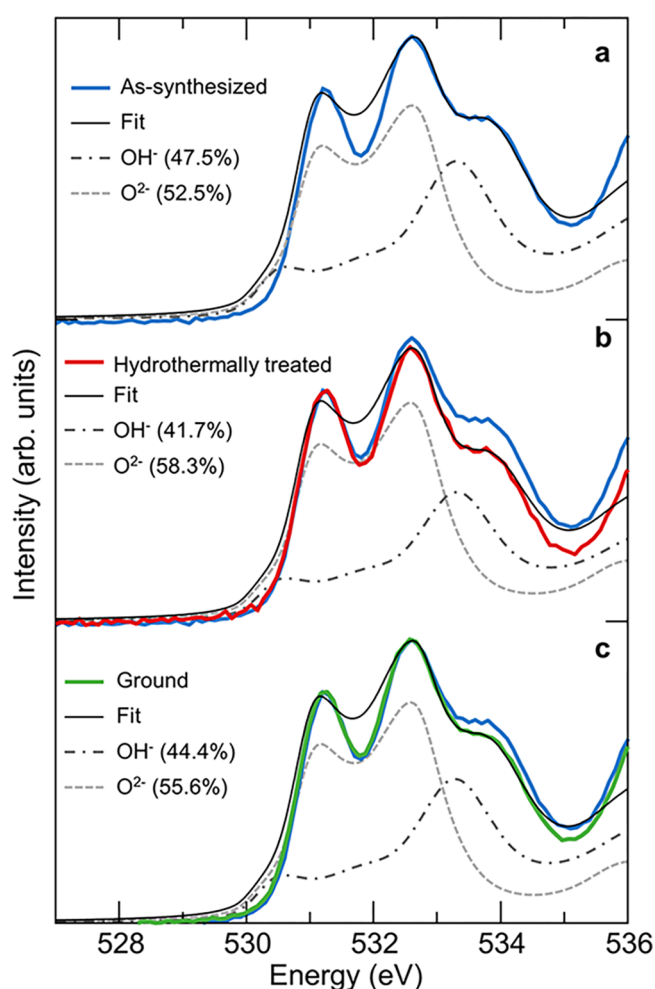


**Figure 6.** O K-edge XAS of goethite after sequential hydrothermal/grinding treatments.

presence of this magnetic moment indicates that the surface is magnetic, likely due to Fe vacancies that disrupt the antiferromagnetic symmetry that would otherwise exist between perfect atomic planes of goethite.<sup>52</sup> The XMCD signal of the hydrothermally treated goethite contains no distinguishable feature, indicating that the magnetic moment is absent, which is consistent with the known bulk antiferromagnetic structure and the hypothesis that hydrothermal

treatment yields a more stoichiometric and crystalline material. After regrinding, the surface magnetic moment, and thus XMCD trace, is largely restored, consistent with reintroduction of Fe vacancies at the surface.

The corresponding O K-edge XAS spectra are illustrated in Figure 6, and analyzed in more detail in SI Figures S11 and S12. The spectral region of primary interest is the pre-edge region between 530 and 535 eV, which is comprised of two  $1s \rightarrow 3d$  excitation doublets, one at lower energy corresponding to  $O^{2-}$  in the goethite surface, and one at higher energy corresponding to  $OH^-$  in the surface.<sup>69</sup> Using DFT, we computed the specific expected shapes of these two doublets and used these theoretical components to perform linear combination fitting (LCF) of the experimentally measured O K-edge spectra for the three goethite samples. We then determined the  $OH^-/O^{2-}$  ratio for the surfaces of each of three goethites. Additionally, the ratio of the measured total integrated Fe L-edge and O K-edge XAS intensities were used to estimate the Fe/O ratios in each of the three surfaces. Here we used the hydrothermally treated goethite as a normalization standard to the bulk ratio of 0.5 under the assumption that this surface is the most stoichiometric within the set. The complete surface compositional results are given in Table 1.

**Table 1.** Summary of Surface Compositional Analyses of Goethite from X-ray Absorption Spectroscopy at the Fe L-Edge and O K-Edge, With the Latter Further Quantified in Terms of  $O^{2-}$  and  $OH^-$ , Using Linear Combination Fitting of the Experimental Spectra with DFT-Based O K-Edge Doublets

	as-synthesized	hydrothermally treated	ground
Fe/O	0.23	0.50 <sup>a</sup>	0.22
$OH^-$	47.45%	41.73%	44.36%
$O^{2-}$	52.55%	58.27%	55.64%
$OH^-/O^{2-}$	0.90	0.72	0.80

<sup>a</sup>To normalize Fe/O ratios based on integrated intensities of separately collected Fe L-edge and O K-edge spectra, all values were scaled proportionally by the factor needed to achieve the idealized 0.50 value for the hydrothermally treated goethite.

The O K-edge spectra for as-synthesized, hydrothermally treated and ground goethites show that the surfaces of the as-synthesized and ground goethite are more hydrous ( $OH^-$  rich relative to  $O^{2-}$ ) than the hydrothermally treated goethite (Figure 6 and Table 1). Note that while the bulk ideal  $OH^-/O^{2-}$  ratio is 50%, the excitation cross sections of the two component spectra are not necessarily equivalent such that a ratio of their integrated intensities could be expected to also correspondingly be 50%; we chose not to normalize these ratios to the ideal value because the trends between samples remain the same in either case. Surfaces of as-synthesized and ground goethite bear comparably lower Fe/O ratios relative to the hydrothermally treated goethite (Table 1), again consistent with the prevalence of Fe vacancies in these two surfaces relative to the hydrothermally treated surface.

Collectively, the observed surface compositional characteristics are consistent with the known behavior of goethite stoichiometry to vary as  $\alpha\text{-Fe}_{1-y/3}\text{O}_{1-y}(\text{OH})_{1+y}$ . Due to excess protons, goethite grown at subhydrothermal temperatures, e.g. 70 °C as used here, tends to be both Fe deficient and correspondingly  $OH^-$ -rich. In contrast, goethite grown hydrothermally tends to be more crystalline and stoichiometric.<sup>43</sup>



Combined, the results from Mössbauer spectroscopy, XAS, and XMCD suggest that particles with fewer defects are less prone to oxidize Fe(II). We propose that the key surface defects are Fe vacancies, which provide sites into which Fe(II) can strongly bind and transfer electrons to lattice Fe(III), propagating a goethite-like surface. Our findings suggest that surface defects play a role in Fe(II)–goethite redox reaction, as predicted by computational chemical modeling.<sup>38–40</sup>

## ■ ENVIRONMENTAL IMPLICATIONS

Here, we provide the first experimental evidence that defects influence the extent of Fe(II)–goethite electron transfer and the composition of the product formed. Our findings indicate that low temperature Fe(III) hydrolysis, a commonly used method for synthesizing goethite, results in goethite particles that have excess hydroxyl/water content and corresponding Fe vacancies that enable Fe(II)–goethite electron transfer. Hydrothermally treating the goethite particles appears to remove defects, inhibit Fe(II)–goethite electron transfer, and alter the composition of the oxidation product. The clear role of defects in enabling Fe(II)–goethite electron transfer resolves the previous discrepancy between multiple experimental observations of Fe(II)–goethite electron transfer<sup>3,4,6,8,10,12,16,17</sup> and computational calculations that suggest Fe(II)–goethite electron transfer is not energetically feasible on structurally perfect surfaces.<sup>38–40</sup>

Our experimental evidence that defects enable Fe(II)–goethite electron transfer raises the question of whether defects influence Fe(II)–catalyzed recrystallization as we and others have proposed that Fe(II)–Fe(III) interfacial electron transfer is an integral step in Fe(II)–catalyzed recrystallization.<sup>7,9,16,70,71</sup> While there has been speculation that mineral surface and structural defects control Fe(II)–catalyzed recrystallization<sup>19,21</sup> experimental data to evaluate this claim is lacking. If Fe(II)–Fe(III) oxide electron transfer controls the extent of Fe oxide recrystallization than our results support the hypothesis that defects play a role in Fe(II)–catalyzed recrystallization. We further speculate that the removal of defects to form a more perfect surface may be the energetic driving force for Fe(II)–catalyzed recrystallization that has continued to elude us. We caution, however, that alternative mechanisms of recrystallization such as solid-state diffusion or pore/void/intergranular diffusion<sup>16,19</sup> have not been ruled out and neither of these mechanisms are likely to be as strongly influenced by electron transfer.

The role of defects in Fe redox chemistry also provides valuable insights into the behavior of Fe oxides in reducing environments. If defects in the form of Fe deficient and OH-rich surfaces enable Fe(II)–goethite electron transfer, then it seems reasonable to suggest that oxidative sorption of Fe(II) at the surface would fill Fe vacancies and anneal some surface defects. Consistent with our suggestion that oxidative sorption of Fe(II) anneals surface defects, we have previously observed less oxidation of sorbed Fe(II) by hematite at high concentrations of Fe(II)<sup>5</sup> as well as reduced extents of hematite recrystallization.<sup>72</sup> Annealing of goethite by oxidative sorption of Fe(II) followed by inhibition of electron transfer may also explain the recent report of decreased goethite recrystallization rates over time.<sup>20</sup> Our hypothesis that oxidative sorption of Fe(II) anneals surface defects is in agreement with results that show addition of Fe(II) inhibits rates of microbial Fe(III) reduction.<sup>73,74</sup> How defects will impact heterogeneous redox process such as contaminant reduction rates,<sup>3,33,34,75–78</sup> and the

observed paradoxical oxidation of As(III) at the Fe(II)–Fe oxide interface, however, remains open to experimental investigation.<sup>8,79,80</sup>

Our work also shows that electron transfer between Fe(II) and goethite is sensitive to diagenetic temperature and can be altered by relatively small changes in the structure. We note that we were only able to observe these changes with surface-sensitive techniques (i.e., XMCD and oxygen XAS). Environmental cycles that include temperature fluctuations, changes in the activity of water, and redox changes can likely reinitialize electron transfer between Fe(II) and goethite, and possibly restart recrystallization by controlling the defect content at the goethite/water interface. The small, subtle changes needed to influence Fe(II)–goethite interaction suggest that in the environment, the extent of this interaction, which also likely underlies Fe(II)–catalyzed recrystallization trace element release and incorporation,<sup>18,35,70</sup> will be coupled to diagenetic history, local redox conditions, and be subject to regeneration via seasonal fluctuations.<sup>34,37</sup>

## ■ ASSOCIATED CONTENT

### ● Supporting Information

The Supporting Information is available free of charge on the ACS Publications website at DOI: 10.1021/acs.est.7b05772.

Details on Mössbauer fitting, discussion on HCl-extracted and oxidized samples as well as additional figures of fitted Mössbauer spectra, Mössbauer spectra of duplicates and extracted samples, SEM and TEM pictures and XRD spectra of the as-synthesized and treated sample (PDF)

## ■ AUTHOR INFORMATION

### Corresponding Author

\*Phone: 319.335.5654; fax: 319.335.5660; e-mail: [michelle-scherer@uiowa.edu](mailto:michelle-scherer@uiowa.edu).

### ORCID

Luiza Notini: 0000-0003-2972-6588

Drew E. Latta: 0000-0001-9414-5590

Michel Sassi: 0000-0003-2582-3735

Kevin M. Rosso: 0000-0002-8474-7720

### Notes

The authors declare no competing financial interest.

## ■ ACKNOWLEDGMENTS

This material is based upon work supported by the U.S. Department of Energy's (DOE) Office of Science, Office of Basic Energy Sciences (BES), Chemical Sciences, Geosciences, and Biosciences Division through its Geosciences program at Pacific Northwest National Laboratory (PNNL). A portion of this research was performed using EMSL, a national scientific user facility sponsored by the DOE Office of Biological and Environmental Research and located at PNNL. The work performed at the Advanced Light Source (ALS) was supported by the Director, Office of Science, BES of the DOE under Contract No. DE-AC02-05CH11231. PNNL is a multiprogram national laboratory operated for DOE by Battelle Memorial Institute under Contract No. DE-AC06-76RLO-1830. Additional support for this work was provided by the National Science Foundation (NSF) through the NSF Division of Chemistry under Grant No. 1347848 and the NSF Division of Graduate Education under Grant No. 1633098.

## ■ REFERENCES

- (1) Stumm, W.; Sulzberger, B. The cycling of iron in natural environments: Considerations based on laboratory studies of heterogeneous redox processes. *Geochim. Cosmochim. Acta* **1992**, *56* (8), 3233–3257.
- (2) Jickells, T. Atmospheric inputs of metals and nutrients to the oceans: their magnitude and effects. *Mar. Chem.* **1995**, *48*, 199–214.
- (3) Williams, A. G. B.; Scherer, M. M. Spectroscopic Evidence for Fe(II)–Fe(III) Electron Transfer at the Iron Oxide–Water Interface. *Environ. Sci. Technol.* **2004**, *38* (18), 4782–4790.
- (4) Silvester, E.; Charlet, L.; Tournassat, C.; Géhin, A.; Grenèche, J.-M.; Liger, E. Redox potential measurements and Mössbauer spectrometry of Fe<sup>II</sup> adsorbed onto Fe<sup>III</sup> (oxyhydr)oxides. *Geochim. Cosmochim. Acta* **2005**, *69* (20), 4801–4815.
- (5) Larese-Casanova, P.; Scherer, M. M. Fe(II) Sorption on Hematite: New Insights Based on Spectroscopic Measurements. *Environ. Sci. Technol.* **2007**, *41* (2), 471–477.
- (6) Cwiertny, D. M.; Handler, R. M.; Schaefer, M. V.; Grassian, V. H.; Scherer, M. M. Interpreting nanoscale size-effects in aggregated Fe-oxide suspensions: Reaction of Fe(II) with Goethite. *Geochim. Cosmochim. Acta* **2008**, *72* (5), 1365–1380.
- (7) Yanina, S. V.; Rosso, K. M. Linked Reactivity at Mineral–Water Interfaces Through Bulk Crystal Conduction. *Science* **2008**, *320* (5873), 218–222.
- (8) Amstatter, K.; Borch, T.; Larese-Casanova, P.; Kappler, A. Redox Transformation of Arsenic by Fe(II)-Activated Goethite ( $\alpha$ -FeOOH). *Environ. Sci. Technol.* **2010**, *44* (1), 102–108.
- (9) Rosso, K. M.; Yanina, S. V.; Gorski, C. A.; Larese-Casanova, P.; Scherer, M. M. Connecting Observations of Hematite ( $\alpha$ -Fe<sub>2</sub>O<sub>3</sub>) Growth Catalyzed by Fe(II). *Environ. Sci. Technol.* **2010**, *44* (1), 61–67.
- (10) Latta, D. E.; Bachman, J. E.; Scherer, M. M. Fe Electron Transfer and Atom Exchange in Goethite: Influence of Al-Substitution and Anion Sorption. *Environ. Sci. Technol.* **2012**, *46* (19), 10614–10623.
- (11) Neumann, A.; Olson, T. L.; Scherer, M. M. Spectroscopic Evidence for Fe(II)–Fe(III) Electron Transfer at Clay Mineral Edge and Basal Sites. *Environ. Sci. Technol.* **2013**, *47* (13), 6969–6977.
- (12) Pasakarnis, T.; McCormick, M. L.; Parkin, G. F.; Thompson, A.; Scherer, M. M. Fe<sup>II</sup>aq–Fe<sup>III</sup>oxide electron transfer and Fe exchange: effect of organic carbon. *Environmental Chemistry* **2015**, *12* (1), 52–63.
- (13) Latta, D. E.; Neumann, A.; Premaratne, W. A. P. J.; Scherer, M. M. Fe(II)–Fe(III) Electron Transfer in a Clay Mineral with Low Fe Content. *ACS Earth and Space Chemistry* **2017**, *1* (4), 197–208.
- (14) Gorski, C. A.; Scherer, M. M. Influence of Magnetite Stoichiometry on Fe<sup>II</sup> Uptake and Nitrobenzene Reduction. *Environ. Sci. Technol.* **2009**, *43* (10), 3675–3680.
- (15) Schaefer, M. V.; Gorski, C. A.; Scherer, M. M. Spectroscopic Evidence for Interfacial Fe(II)–Fe(III) Electron Transfer in a Clay Mineral. *Environ. Sci. Technol.* **2011**, *45* (2), 540–545.
- (16) Handler, R. M.; Beard, B. L.; Johnson, C. M.; Scherer, M. M. Atom Exchange between Aqueous Fe(II) and Goethite: An Fe Isotope Tracer Study. *Environ. Sci. Technol.* **2009**, *43* (4), 1102–1107.
- (17) Handler, R. M.; Frierdich, A. J.; Johnson, C. M.; Rosso, K. M.; Beard, B. L.; Wang, C.; Latta, D. E.; Neumann, A.; Pasakarnis, T.; Premaratne, W. A. P. J.; Scherer, M. M. Fe(II)-Catalyzed Recrystallization of Goethite Revisited. *Environ. Sci. Technol.* **2014**, *48* (19), 11302–11311.
- (18) Latta, D. E.; Gorski, C. A.; Scherer, M. M. Influence of Fe<sup>2+</sup>-catalyzed iron oxide recrystallization on metal cycling. *Biochem. Soc. Trans.* **2012**, *40* (6), 1191–1197.
- (19) Gorski, C. A.; Fantle, M. S. Stable mineral recrystallization in low temperature aqueous systems: A critical review. *Geochim. Cosmochim. Acta* **2017**, *198*, 439–465.
- (20) Joshi, P.; Fantle, M. S.; Larese-Casanova, P.; Gorski, C. A. Susceptibility of Goethite to Fe<sup>2+</sup>-Catalyzed Recrystallization over Time. *Environ. Sci. Technol.* **2017**, *51* 1168110.1021/acs.est.7b02603
- (21) Joshi, P.; Gorski, C. A. Anisotropic Morphological Changes in Goethite during Fe<sup>2+</sup>-Catalyzed Recrystallization. *Environ. Sci. Technol.* **2016**, *50* (14), 7315–7324.
- (22) Neumann, A.; Wu, L.; Li, W.; Beard, B. L.; Johnson, C. M.; Rosso, K. M.; Frierdich, A. J.; Scherer, M. M. Atom Exchange between Aqueous Fe(II) and Structural Fe in Clay Minerals. *Environ. Sci. Technol.* **2015**, *49* (5), 2786–2795.
- (23) Gorski, C. A.; Handler, R. M.; Beard, B. L.; Pasakarnis, T.; Johnson, C. M.; Scherer, M. M. Fe Atom Exchange between Aqueous Fe<sup>2+</sup> and Magnetite. *Environ. Sci. Technol.* **2012**, *46* (22), 12399–12407.
- (24) Murray, G. C.; Hesterberg, D. Iron and phosphate dissolution during abiotic reduction of ferrihydrite-boehmite mixtures. *Soil Sci. Soc. Am. J.* **2006**, *70* (4), 1318–1327.
- (25) Matocha, C. J.; Dhakal, P.; Pyzola, S. M., Chapter Four - The Role of Abiotic and Coupled Biotic/Abiotic Mineral Controlled Redox Processes in Nitrate Reduction. In *Advances in Agronomy*; Donald, L. S., Ed.; Academic Press, 2012; Vol. 115, pp 181–214.
- (26) Van Cleemput, O. Subsoils: chemo- and biological denitrification, N<sub>2</sub>O and N<sub>2</sub> emissions. *Nutr. Cycling Agroecosyst.* **1998**, *52* (2–3), 187–194.
- (27) Ernsten, V. Reduction of Nitrate by Fe<sup>2+</sup> in Clay Minerals. *Clays Clay Miner.* **1996**, *44* (5), 599–608.
- (28) Colombo, C.; Palumbo, G.; He, J.-Z.; Pinton, R.; Cesco, S. Review on iron availability in soil: interaction of Fe minerals, plants, and microbes. *J. Soils Sediments* **2014**, *14* (3), 538–548.
- (29) Weber, K. A.; Achenbach, L. A.; Coates, J. D. Microorganisms pumping iron: anaerobic microbial iron oxidation and reduction. *Nat. Rev. Microbiol.* **2006**, *4* (10), 752–764.
- (30) Chun, C. L.; Hozalski, R. M.; Arnold, W. A. Degradation of Drinking Water Disinfection Byproducts by Synthetic Goethite and Magnetite. *Environ. Sci. Technol.* **2005**, *39* (21), 8525–8532.
- (31) Peretyazhko, T.; Zachara, J. M.; Heald, S. M.; Jeon, B. H.; Kukkadapu, R. K.; Liu, C.; Moore, D.; Resch, C. T. Heterogeneous reduction of Tc(VII) by Fe(II) at the solid–water interface. *Geochim. Cosmochim. Acta* **2008**, *72* (6), 1521–1539.
- (32) Latta, D. E.; Boyanov, M. I.; Kemner, K. M.; O'Loughlin, E. J.; Scherer, M. M. Abiotic reduction of uranium by Fe (II) in soil. *Appl. Geochem.* **2012**, *27* (8), 1512–1524.
- (33) Stemig, A. M.; Do, T. A.; Yuwono, V. M.; Arnold, W. A.; Penn, R. L. Goethite nanoparticle aggregation: effects of buffers, metal ions, and 4-chloronitrobenzene reduction. *Environ. Sci.: Nano* **2014**, *1* (5), 478–487.
- (34) Tomaszewski, E. J.; Lee, S.; Rudolph, J.; Xu, H.; Ginder-Vogel, M. The reactivity of Fe(II) associated with goethite formed during short redox cycles toward Cr(VI) reduction under oxic conditions. *Chem. Geol.* **2017**, *464*, 101–109.
- (35) Frierdich, A. J.; Catalano, J. G. Fe(II)-Mediated Reduction and Repartitioning of Structurally Incorporated Cu, Co, and Mn in Iron Oxides. *Environ. Sci. Technol.* **2012**, *46* (20), 11070–11077.
- (36) Pedersen, H. D.; Postma, D.; Jakobsen, R.; Larsen, O. Fast transformation of iron oxyhydroxides by the catalytic action of aqueous Fe(II). *Geochim. Cosmochim. Acta* **2005**, *69* (16), 3967–3977.
- (37) Johnson, C. M.; Beard, B. L.; Roden, E. E. The Iron Isotope Fingerprints of Redox and Biogeochemical Cycling in Modern and Ancient Earth. *Annu. Rev. Earth Planet. Sci.* **2008**, *36* (1), 457–493.
- (38) Alexandrov, V.; Rosso, K. M. Ab initio modeling of Fe(II) adsorption and interfacial electron transfer at goethite ( $\alpha$ -FeOOH) surfaces. *Phys. Chem. Chem. Phys.* **2015**, *17* (22), 14518–14531.
- (39) Kubicki, J. D.; Tunega, D.; Kraemer, S., A density functional theory investigation of oxalate and Fe(II) adsorption onto the (010) goethite surface with implications for ligand- and reduction-promoted dissolution. *Chem. Geol.* **2016**, *464* 1410.1016/j.chemgeo.2016.08.010
- (40) Russell, B.; Payne, M.; Ciacchi, L. C. Density functional theory study of Fe(II) adsorption and oxidation on goethite surfaces. *Phys. Rev. B: Condens. Matter Mater. Phys.* **2009**, *79* (16), 165101.
- (41) Zarzycki, P.; Kerisit, S.; Rosso, K. M. Molecular Dynamics Study of Fe(II) Adsorption, Electron Exchange, and Mobility at Goethite ( $\alpha$ -FeOOH) Surfaces. *J. Phys. Chem. C* **2015**, *119* (6), 3111–3123.



- (42) Soltis, J. A.; Schwartzberg, A. M.; Zarzycki, P.; Penn, R. L.; Rosso, K. M.; Gilbert, B. Electron Mobility and Trapping in Ferrihydrite Nanoparticles. *ACS Earth and Space Chemistry* **2017**, *1* (4), 216–226.
- (43) Schwertmann, U.; Cambier, P.; Murad, E. Properties of goethites of varying crystallinity. *Clays Clay Miner.* **1985**, *33* (5), 369–378.
- (44) Strauss, R.; Brümmer, G. W.; Barrow, N. J. Effects of crystallinity of goethite: I. Preparation and properties of goethites of differing crystallinity. *Eur. J. Soil Sci.* **1997**, *48* (1), 87–99.
- (45) Madsen, D. E.; Cervera-Gontard, L.; Kasama, T.; Dunin-Borkowski, R. E.; Koch, C. B.; Hansen, M. F.; Frandsen, C.; Mørup, S. Magnetic fluctuations in nanosized goethite ( $\alpha$ -FeOOH) grains. *J. Phys.: Condens. Matter* **2009**, *21* (1), 016007.
- (46) Barrero, C. A.; Betancur, J. D.; Greneche, J. M.; Goya, G. F.; Berquó, T. S. Magnetism in non-stoichiometric goethite of varying total water content and surface area. *Geophys. J. Int.* **2006**, *164* (2), 331–339.
- (47) Bocquet, S.; Hill, A. Correlation of Néel temperature and vacancy defects in fine-particle goethites. *Phys. Chem. Miner.* **1995**, *22* (8), 524–528.
- (48) Cornell, R. M.; Schwertmann, U., Crystal Structure. In *The Iron Oxides*; Wiley-VCH Verlag GmbH & Co. KGaA, 2004; pp 9–38.
- (49) De Yoreo, J. J.; Gilbert, P. U.; Sommerdijk, N. A.; Penn, R. L.; Whitlam, S.; Joester, D.; Zhang, H.; Rimer, J. D.; Navrotsky, A.; Banfield, J. F. Crystallization by particle attachment in synthetic, biogenic, and geologic environments. *Science* **2015**, *349* (6247), aab6760.
- (50) Penn, R. L.; Banfield, J. F. Imperfect Oriented Attachment: Dislocation Generation in Defect-Free Nanocrystals. *Science* **1998**, *281* (5379), 969–971.
- (51) Banfield, J. F.; Welch, S. A.; Zhang, H.; Ebert, T. T.; Penn, R. L. Aggregation-Based Crystal Growth and Microstructure Development in Natural Iron Oxyhydroxide Biomineralization Products. *Science* **2000**, *289* (5480), 751–754.
- (52) Brož, D.; Sedláč, B. Surface ferrimagnetism of synthetic goethite. *J. Magn. Magn. Mater.* **1991**, *102* (1), 103–108.
- (53) Bocquet, S.; Pollard, R. J.; Cashion, J. D. Dynamic magnetic phenomena in fine-particle goethite. *Phys. Rev. B: Condens. Matter Mater. Phys.* **1992**, *46* (18), 11657–11664.
- (54) Stacey, F. D.; Banerjee, S. K., Chapter 2 - Magnetic Minerals. In *Developments in Solid Earth Geophysics*; Frank D, S.; Subir K, B., Eds.; Elsevier: 1974; Vol. 5, pp 25–40.
- (55) Özdemir, Ö.; Dunlop, D. J. Thermoremanence and Néel temperature of goethite. *Geophys. Res. Lett.* **1996**, *23* (9), 921–924.
- (56) Fischer, L.; Mühlen, E. Z.; Brümmer, G. W.; Niehus, H. Atomic force microscopy (AFM) investigations of the surface topography of a multidomain porous goethite. *Eur. J. Soil Sci.* **1996**, *47* (3), 329–334.
- (57) Schwertmann, U.; Cornell, R. M. Goethite. In *Iron Oxides in the Laboratory*; Wiley-VCH Verlag GmbH, 2007; pp 67–92.
- (58) Good, N. E.; Winget, G. D.; Winter, W.; Connolly, T. N.; Izawa, S.; Singh, R. M. M. Hydrogen Ion Buffers for Biological Research\*. *Biochemistry* **1966**, *5* (2), 467–477.
- (59) Tamura, H.; Goto, K.; Yotsuyanagi, T.; Nagayama, M. Spectrophotometric determination of iron(II) with 1,10-phenanthroline in the presence of large amounts of iron(III). *Talanta* **1974**, *21* (4), 314–318.
- (60) Rancourt, D. G.; Ping, J. Y. Voigt-based methods for arbitrary-shape static hyperfine parameter distributions in Mössbauer spectroscopy. *Nucl. Instrum. Methods Phys. Res., Sect. B* **1991**, *58* (1), 85–97.
- (61) Joly, Y. X-ray absorption near-edge structure calculations beyond the muffin-tin approximation. *Phys. Rev. B: Condens. Matter Mater. Phys.* **2001**, *63* (12), 125120.
- (62) Hedin, L.; Lundqvist, B. I. Explicit local exchange-correlation potentials. *J. Phys. C: Solid State Phys.* **1971**, *4* (14), 2064.
- (63) Piepenbrock, A.; Schröder, C.; Kappler, A. Electron transfer from humic substances to biogenic and abiogenic Fe (III) oxyhydroxide minerals. *Environ. Sci. Technol.* **2014**, *48* (3), 1656–1664.
- (64) Buchholz, A.; Laskov, C.; Haderlein, S. B. Effects of Zwitterionic Buffers on Sorption of Ferrous Iron at Goethite and Its Oxidation by  $\text{CCl}_4$ . *Environ. Sci. Technol.* **2011**, *45* (8), 3355–3360.
- (65) Cornell, R. M.; Schwertmann, U. Formation. In *The Iron Oxides*; Wiley-VCH Verlag GmbH & Co. KGaA, 2004; pp 345–364.
- (66) Burns, R. G. Intervalence transitions in mixed valence minerals of iron and titanium. *Annu. Rev. Earth Planet. Sci.* **1981**, *9* (1), 345–383.
- (67) Liu, J.; Pearce, C. I.; Liu, C.; Wang, Z.; Shi, L.; Arenholz, E.; Rosso, K. M.  $\text{Fe}_{3-x}\text{Ti}_x\text{O}_4$  Nanoparticles as Tunable Probes of Microbial Metal Oxidation. *J. Am. Chem. Soc.* **2013**, *135* (24), 8896–8907.
- (68) Sassi, M.; Pearce, C. I.; Bagus, P. S.; Arenholz, E.; Rosso, K. M., First Principles Fe  $L_{2,3}$ -Edge and O K-Edge XANES and XMCD Spectra for Iron Oxides. *J. Phys. Chem. A* **2017**, *121* 761310.1021/acs.jpca.7b08392
- (69) Gilbert, B.; Erbs, J. J.; Penn, R. L.; Petkov, V.; Spagnoli, D.; Waychunas, G. A. A disordered nanoparticle model for 6-line ferrihydrite. *Am. Mineral.* **2013**, *98* (8–9), 1465–1476.
- (70) Frierdich, A. J.; Catalano, J. G. Controls on Fe(II)-Activated Trace Element Release from Goethite and Hematite. *Environ. Sci. Technol.* **2012**, *46* (3), 1519–1526.
- (71) Jones, A. M.; Collins, R. N.; Rose, J.; Waite, T. D. The effect of silica and natural organic matter on the Fe(II)-catalysed transformation and reactivity of Fe(III) minerals. *Geochim. Cosmochim. Acta* **2009**, *73* (15), 4409–4422.
- (72) Frierdich, A. J.; Helgeson, M.; Liu, C.; Wang, C.; Rosso, K. M.; Scherer, M. M. Iron atom exchange between hematite and aqueous Fe(II). *Environ. Sci. Technol.* **2015**, *49* (14), 8479–8486.
- (73) Roden, E. E.; Urrutia, M. M.; Mann, C. J. Bacterial Reductive Dissolution of Crystalline Fe(III) Oxide in Continuous-Flow Column Reactors. *Appl. Environ. Microbiol.* **2000**, *66* (3), 1062–1065.
- (74) Roden, E. E.; Urrutia, M. M. Influence of biogenic Fe (II) on bacterial crystalline Fe (III) oxide reduction. *Geomicrobiol. J.* **2002**, *19* (2), 209–251.
- (75) Klausen, J.; Trober, S. P.; Haderlein, S. B.; Schwarzenbach, R. P. Reduction of substituted nitrobenzenes by Fe(II) in aqueous mineral suspensions. *Environ. Sci. Technol.* **1995**, *29* (9), 2396–2404.
- (76) Amonette, J. E.; Workman, D. J.; Kennedy, D. W.; Fruchter, J. S.; Gorby, Y. A. Dechlorination of carbon tetrachloride by Fe(II) associated with goethite. *Environ. Sci. Technol.* **2000**, *34* (21), 4606–4613.
- (77) Gorski, C. A.; Edwards, R.; Sander, M.; Hofstetter, T. B.; Stewart, S. M. Thermodynamic Characterization of Iron Oxide–Aqueous  $\text{Fe}^{2+}$  Redox Couples. *Environ. Sci. Technol.* **2016**, *50* (16), 8538–8547.
- (78) Fan, D.; Bradley, M. J.; Hinkle, A. W.; Johnson, R. L.; Tratnyek, P. G. Chemical Reactivity Probes for Assessing Abiotic Natural Attenuation by Reducing Iron Minerals. *Environ. Sci. Technol.* **2016**, *50* (4), 1868–1876.
- (79) Wang, L.; Giammar, D. E. Effects of pH, dissolved oxygen, and aqueous ferrous iron on the adsorption of arsenic to lepidocrocite. *J. Colloid Interface Sci.* **2015**, *448*, 331–338.
- (80) Ilgen, A. G.; Kruichak, J.; Artyushkova, K.; Newville, M.; Sun, C. -J., Redox transformations of As and Se at the surfaces of natural and synthetic ferric nontronites: role of structural and adsorbed Fe(II). *Environ. Sci. Technol.* **2017**, *51* 1110510.1021/acs.est.7b03058